Journal of Contaminant Hydrology, 14 (1993) 163–192
Elsevier Science Publishers B.V., Amsterdam

Fluid flow and solute transport in a network of channels

Luis Moreno and Ivars Neretnieks

Department of Chemical Engineering, Royal Institute of Technology, S-100 44 Stockholm, Sweden

(Received March 2, 1993; revised and accepted June 25, 1993)

ABSTRACT

Moreno, L. and Neretnieks, I., 1993. Fluid flow and solute transport in a network of channels. J. Contam. Hydrol., 14: 163–192.

A new model to describe flow and transport in fractured rocks is proposed. It is based on the concept of a network of channels. The individual channel members are given stochastically selected conductances and volumes. Flow-rate calculations have been performed. For large standard deviations in conductances, channeling becomes pronounced with most of the water flowing in a few paths. The effluent patterns and flow-rate distributions obtained in the simulations have been compared to three field measurements in drifts and tunnels of flow-rate distributions. Standard deviations of channel conductances were between 1.6 and $\geqslant 2.4$ in some cases. A particle-following technique was used to simulate solute transport in the network. Non-sorbing as well as sorbing solute transport can be simulated. By using a special technique, solutes that diffuse into the rock matrix can also be simulated.

INTRODUCTION AND BACKGROUND

In Sweden it is planned to site the repository for spent nuclear fuel at $\sim$ 500-m depth in crystalline rock, e.g. granite. These rocks are fractured and water flows in sparse channels in the fractures. Water flow rates are low at these depths, typically < 0.1 L m^{-2} yr^{-1}. Most of the radionuclides of interest sorb strongly onto the rock minerals and will be considerably retarded, in relation to the water velocity, by this interaction.

In this paper we develop a new model for solute transport in sparsely fractured rock. We also explore some of the properties of the model that affect radionuclide migration. Furthermore, we attempt to estimate values for the important parameters from large-scale field experiments and observations.

Flow and solute transport in fractured rock has been found to be poorly

0169-7722/93/$06.00

NOTATION

List of symbols used in the text

Symbol	Description	Unit
A	area	(m^2)
a	wetted surface	(m^2 m^{-3})
C	conductance	(m^4 s kg^{-1})
c	concentration	(mol m^{-3})
D_e	effective diffusion coefficient	(m^2 s^{-1})
D_{bh}	borehole diameter	(m)
K_d	sorption coefficient	(m^3 kg^{-1})
L	length	(m)
P	pressure	(kg m^{-1} s^{-2})
Pe	Péclet number	
Q	water flow rate	(m^3 s^{-1})
W	channel width	(m)
r	radial distance	(m)
t_w	water residence time	(s)
Z	channel length	(m)
α	angle	(°)
δ	aperture	(m)
ϵ	porosity	
μ_o	mean logarithm of conductance	
ρ_p	density of bulk rock	(kg m^{-3})
σ	standard deviation in the log-normal distribution of conductances	
σ_t	standard deviation in the residence time distribution	(s)

described by the advection–dispersion concept and equations. Field observations show that there are strong channeling effects and that when attempts are made to evaluate the dispersion coefficient, it appears to increase with distance (Neretnieks et al., 1987; Abelin et al., 1991b). Field observations in drifts and tunnels also show that flow channels are sparse and that the flow-rate distribution is very large among channels (Neretnieks et al., 1987). For short distances, it has been proposed that the flow and solute transport might better be described as taking place in a bundle of independent channels (Neretnieks et al., 1987). For longer distances, channels have a greater chance of meeting and a network concept seems more appropriate. For very long distances, it is conceivable that the mixing between channels is large enough for the transport to behave as described by the advection–dispersion model. This does not seem to have been observed in fractured rocks so far.

Fracture network models have been proposed and tested on field data (Robinson, 1984; Long et al., 1985; Dverstorp and Andersson, 1989; Dershowitz et al., 1991) for flow calculations and in some cases also for tracer

transport (Cacas et al., 1990b; Dverstorp, 1991). These models need information on fracture trace lengths, orientations, frequencies and transmissivities, plus some assumptions, that are difficult to prove. In the end, they have to be calibrated to field observations.

In this paper we attempt a simpler approach, and assume that flow and solute transport can be described as taking place in a network of channels. This simplification allows us to develop a simple model that does not need very detailed information. Data can be obtained from borehole transmissivity measurements and observations on fracture widths. Calibrations can be made with observations in drifts and tunnels. One important aspect of the model is that it is simple enough to accommodate the transport of sorbing solutes, especially those that diffuse into the rock matrix and sorb in the interior of the matrix. This is very important when assessing retardation of radionuclides, which may escape from repositories for nuclear waste. Below, we summarize some observations that have been the basis for the formulation of this model.

Abelin et al. (1985) analyzed flow and solute movement in three natural fractures intersecting tunnels in the granite in the Stripa mine, Sweden. They found that the fractures were closed or very tight, with few open parts between the areas where two fracture surfaces are in contact. Observations in drifts and tunnels strengthen this impression (Neretnieks, 1987; Neretnieks et al., 1987). In two investigations (Neretnieks, 1987; Abelin et al., 1991a, b) it was found that fracture intersections often make up high flow-rate conduits.

In the tracer test experiment performed in the Stripa mine by Abelin et al. (1991a, b), it was found that water flows into the drift with a very uneven spatial distribution. The results also show that the tracers are unevenly distributed in the drift. Very different concentrations were found in sheets near each other. Low values alternate with high values in nearby locations. In some cases, much of the tracer was found in locations far away from the injection hole.

Detailed observations of flow distributions in two other long drifts and tunnels, Kymmen, western Sweden (Palmqvist and Stanfors, 1987) and the repository for low and intermediate waste, called SFR, Sweden (Neretnieks et al., 1987), show that the water outflow occurs in narrow channels, most of them < 10 cm wide. The channel density is ~ 1 per 20–100 m^2. Experiments that specifically aim to study channeling in individual natural fractures on the scale of 2–2.5 m in the Stripa mine (Abelin et al., 1990) also show that water is conducted in only a small part of a fracture. Channels have typical widths of < 10 cm. Hydraulic conductivities measured in the fracture planes show that there are very strong variations in conductivity in the plane of the fractures.

Porous medium models cannot describe this uneven flow distribution. Network models have been used to describe the flow-rate distribution in the

Stripa experiment (Geier et al., 1990; Herbert and Splawski, 1990; Dverstorp, 1991; Herbert et al., 1991). They describe the stochastic nature of the areal flow distribution but do not account for the channeling nature of the flow. None of the models have addressed the question of the interaction of solutes with the rock surfaces. Nor have any of the models accounted for the observations (Neretnieks, 1987; Abelin et al., 1990) that fracture intersections play an important role in conducting the water solutes.

In a recent study, it was assumed that the flow in fractures that intersect each other can be described as the flow through channels in the planes of the fractures (Cacas et al., 1990a). These channels connect the centres of the fractures through a point at the intersection line between the fractures. The fracture network may then be simplified to a network of connected channels.

One of the drawbacks of these models is that they need a large and very detailed data on fracture orientations, fracture size distributions and fracture conductivity distributions. A number of assumptions must also be made in interpreting the field observations to translate them into the data used in the models. Many of the assumptions are dubious and difficult to validate. One additional difficulty is the necessity of using only a small fraction of the real number of fractures in the simulations, because even the largest of today's computers cannot handle more information. The models with all their built-in assumptions must finally be validated by comparison with field data. The model described here needs much less data but also needs to be validated by field observations.

CONCEPTUAL MODEL

In our approach a three-dimensional (3-D) channel network model is developed. It can account for the stochastic nature of the flow distribution, the channeling nature of the flow and the interaction of reactive solutes with the flow-wetted rock surfaces. The solutes in the channels can also diffuse into and out of the rock matrix.

To avoid many of the difficulties that fracture networks exhibit, we choose a different starting approach. It is assumed that the flow paths make up a channel network in the rock. Every channel member can connect to any number of other channel members, but we choose an upper limit of six members intersecting at a point, for reasons that are described below. Some of these channel members may have a conductivity that is so low that no connection is made.

The use of six channel members is partly based on the observation that both fracture intersection and channels in the fracture planes play an important role in conducting flow. For two fractures that intersect, there will be one channel in every fracture plane that may continue

over the intersection line with the other fracture. In this way, up to four members in the fracture plane may intersect at one node. For those intersections where the fracture intersection itself is conducting, two more members may be added, forming a 6-member intersection. If there is more than one channel in a fracture, an independent intersection point will exist.

Although the model concept is based on the above considerations, this does not mean that we consider a channel to lie only in one fracture or at a fracture intersection. A channel in our concept may have been formed by individual channel members in series. Thus a channel may consist of 1, 2, 3 or even more channel members. The actual number is not very important, as the properties of the channels will be obtained by calibration to field measurements. It would be helpful if many channel members could be combined in this manner, provided the important flow and transport properties were maintained, because the computation increases considerably with the total number of channels used in the model.

For visualization purposes, the network is depicted as a 3-D rectangular grid. The hydraulic properties of the members can be generated by including the effects of channel members of different lengths, different hydraulic conductivities and other properties of interest. It is easy to vary the channel member density in different regions (e.g., along fracture zones) and to include effects of anisotropy in a simplified manner. In this paper, we develop and test only some important basic properties of the model. They include the ability to describe the uneven spatial distribution of flow, the residence time distributions of tracers, and the retardation due to matrix diffusion and sorption in the rock matrix.

We do not think of the channels as necessarily being clearly identifiable physical features. In a fracture with varying apertures, the water will trace out different paths, depending on the gradient that exists at a given moment. When the conductivity variations are large, there will only be one or a few paths where most of the water flows. This has been found in simulations (Moreno et al., 1988, 1990) as well as in the field (Abelin et al., 1990). The flow paths may also be actual physical channels along fracture intersections or where dissolution processes have formed channels. They may have properties that vary along the flow path, but an average conductivity, volume and flow-wetted surface may be assigned to every channel member in the model.

All properties of the channel members used in our model are thought to have a stochastic nature. The average transmissivity along a member and its length define the conductance. This is the only entity needed to calculate the flow, if the pressure difference between the two ends of the member is known. If the residence time is to be calculated for non-interacting solutes then the volume of the channel members is needed as well. For solutes that can sorb on

the rock, the "flow-wetted" surface area is also needed (Neretnieks, 1980). If the rock matrix is porous and the solutes have access to the interior porosity, the matrix diffusion properties must be known as well. We assume that it is possible to average these properties along a channel member. We also assume, in the present paper, that there is ideal mixing at channel intersections.

The residence time distribution (RTD) is often described in terms of a mean residence time and dispersion. These are obtained from the first and second moments of the RTD. Higher moments, which describe exceptionally long tails or early arrivals, are usually not considered. Although early arrivals, in particular, may play an important role for decaying radionuclides.

There are several mechanisms that cause dispersion of tracers: dispersion in the individual members of the network, dispersion caused by increase in the spread of residence times due to different velocities in the channels, and spreading caused by matrix diffusion effects. In preliminary calculations, we found that the dispersion in the individual members is negligible compared to the two other causes. This was also found by Cacas et al. (1990b), and will not be discussed further in this study.

Mixing at intersections will also influence the RTD of the network. Several possible reasonable assumptions can be made of the mixing processes (Robinson, 1984; Smith et al., 1987), but none have been actually tested in real networks. We will only use the full mixing assumption in this paper.

Matrix diffusion effects and sorption in the interior of the matrix are assumed to be active, and to be a Fickian process (Neretnieks, 1980).

Both linear and convergent flow are simulated. The latter one to account for the inflow to a tunnel, such as in Stripa, and to compare with the flow-rate distribution there. Tracer transport is simulated in the same networks. For tracer transport, additional information on channel volumes and flow-wetted surfaces is needed. No independent data on this are available, and therefore various assumptions are used and compared with the field results.

CALCULATION PROCEDURES

Generation of network

The use of a 3-D rectangular network does not mean that the channel members are of equal length or that they form such a network: it is only a simple way of visualizing the network. Each member of the network is assigned a hydraulic conductance. The orientation and location of the members only become important when they are compared with real geometry.

The flow calculations only need the information on the conductances of the channel members and the boundary conditions. The conductance is defined as

the ratio between the flow in a channel member and the pressure difference between its ends. When solute transport is included, the volume of the member has to be known. If sorption onto the fracture surface or diffusion into the matrix will be included in the model, the surface area of the flow-wetted surface must also be included. Then some properties of the rock are needed as well, such as rock matrix porosity, diffusivity, and sorption capacity for sorbing species.

In the present simulations, the conductances of the channel members are assumed to be log-normally distributed, with mean μ_0 and standard deviation σ_c. It is also assumed that the conductances are not correlated in space. The volume will be estimated by using various assumptions, due to the lack of data.

Fig. 1 shows a schematic view of the mesh used in this paper. An outline of the approach used to calculate the fluid flow and solute transport through the network of members is presented below. The method is described in more detail in Moreno et al. (1988).

Fluid flow calculations

For laminar conditions, the flow through a channel member is proportional to the pressure gradient. The flow between two points i and j may be written as:

$$Q_{ij} = C_{ij}(P_j - P_i) \tag{1}$$

where C_{ij} is the conductance connecting the nodes i and j. The pressure field is

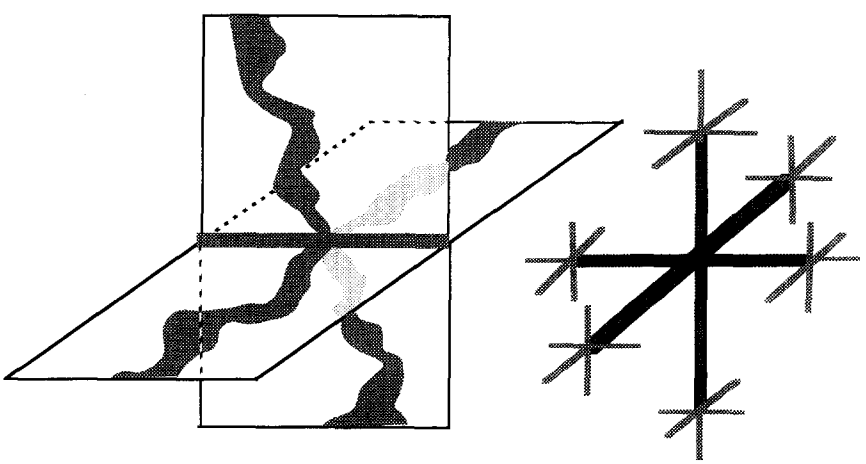

Fig. 1. At a fracture intersection up to six channel members may intersect.

calculated by writing the mass balance at each intersection point:

$$\sum_j Q_{ij} = 0 \qquad \text{for all } i \tag{2}$$

The solution of this system of equations yields the pressure at each node. Flow between adjacent nodes is then calculated by using Eq. 1.

Solute transport calculations

The solute transport is simulated by using a particle-following technique (Robinson, 1984; Moreno et al., 1988). Many particles are introduced, one at a time, into the known flow field at one or more locations. Particles arriving to an intersection are distributed in the outlet channel members with a probability proportional to their flow rates. This is equivalent to assuming total mixing at the intersections. Each individual particle is followed through the network. The residence time in a given channel for non-sorbing tracers is determined by the flow through the channel member and by its volume. The residence time of an individual particle along the whole path is determined as the sum of residence times in every channel member that the particle has traversed. The residence time distribution is then obtained from the residence times of a multitude of individual particle runs.

From the RTD, the mean residence time and variance can be calculated. They may be used to determine the Péclet number, which is a dimensionless measure of the dispersivity (Levenspiel, 1972).

$$2/\mathrm{Pe} = \sigma_t^2/t_w^2 \tag{3}$$

When dispersion in the channel and/or diffusion into the rock matrix are considered, different particles in the same channel member will have different residence times. Here, residence times for the particles may be described by the RTD of the particles, expressed as a probability density function, pdf. It may be thought of as the outlet concentration for a pulse injection. If this curve is integrated over all the possible residence times, the cumulative distribution of the residence times is obtained.

When diffusion from the moving water into and out of the rock matrix takes place, a particle may reside in the matrix for some time in addition to its residence time in the water in the channel member. For a flat channel from which the diffusion, in a semi-infinite medium, is perpendicular to the channel surface, a simple analytical solution is available for the RTD. The cumulative curve, F, for the residence times is obtained as (Carslaw and Jaeger, 1959):

$$F = \mathrm{erfc}\,[(K_d D_e \rho_p)^{0.5} t_w/(t - t_w)^{0.5}\delta] \tag{4}$$

for times greater than the water-plug-flow residence time t_w. Otherwise the

value is zero. Eq. 4 considers only advection in the channel and diffusion into the rock matrix. Longitudinal dispersion is neglected. (See Notation for definition of symbols.)

For a rectangular channel member, the water-plug-flow residence time is obtained from the ratio between the channel volume and the flow rate through it. It may be calculated by $LW\delta/Q$. Introducing this expression into Eq. 4 yields:

$$F = \text{erfc}\left[(K_d D_e \rho_p)^{0.5} LW/(t - t_w)^{0.5} Q\right] \tag{5}$$

For particle following, we adopt the technique used by Yamashita and Kimura (1990). The travel time for each particle in a channel member is determined by choosing a uniform random number in the interval [0,1]. The travel time for the particle, t, is then calculated by solving for t in the following equation:

$$[R]_0^1 = \text{erfc}\left[(K_d D_e \rho_p)^{0.5} LW/(t - t_w)^{0.5} Q\right] \tag{6}$$

SOME PROPERTIES OF THE MODEL

The simulated domain is a cubic grid with 20 channel members in each direction. The pressure gradient is imposed perpendicularly to one side. No-flow conditions are imposed on the four sides parallel to the pressure gradient. The outflow is through the 400 channels in the low-pressure side. Grids with a larger number of channel members were also simulated.

Flow-rate distributions

Fig. 2 shows the number of channels, of the 400 at the outflow face of the cubic grid, which carry a given flow rate (relative) for two σ_c. Note that the flow rate decreases to the right in the graph. The flow rates have been grouped in "bins" with the upper bound twice as large as the lower bound. This forms a geometric progression with a factor of 2 between the bins. This mode of representation has been chosen because in practice the larger channels will always be seen, whereas the measurement limit will determine the smallest flow rates that can be observed. In field observations, only the flow rates in the 6–8 bins with the largest flow rates may be used for calibration purposes. This means flow rates in 2–3 orders of magnitude. In histograms showing the fraction of flow in a given interval, only the largest flow rates contribute significantly to the total flow. Fig. 3 shows the cumulative fraction of flow for flow rates less than a given value, for two σ_c. The total flow is normalized to the total flow in the 8 largest intervals. The contribution of the interval with

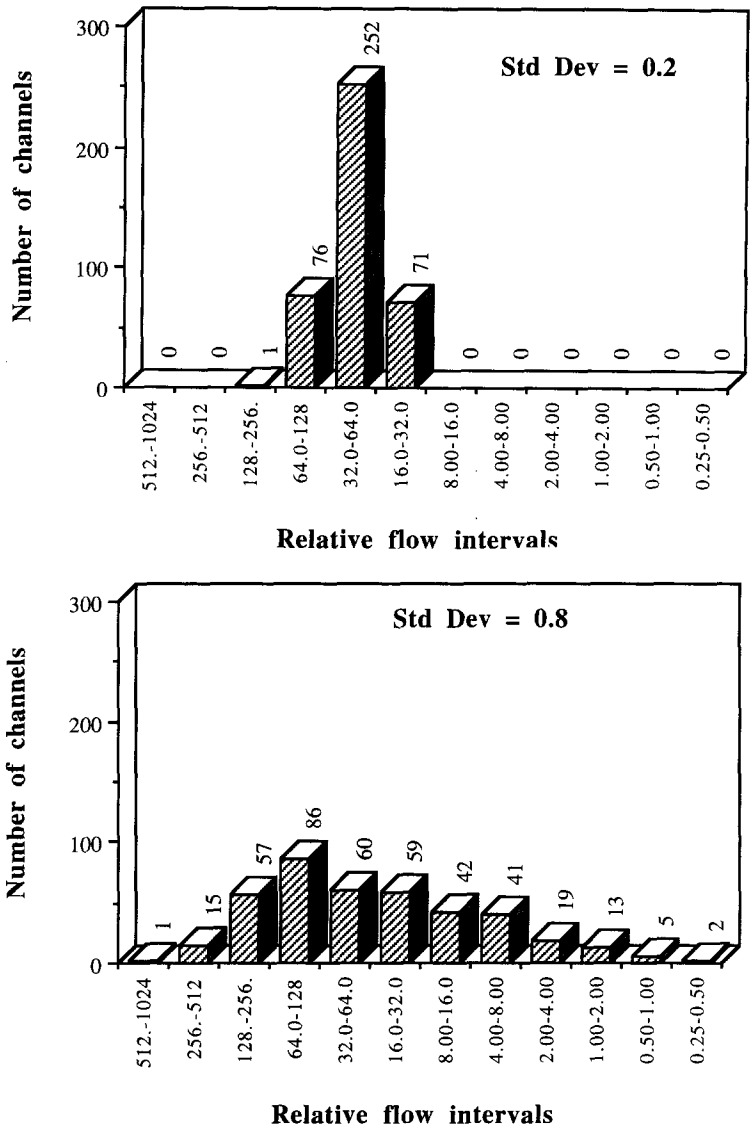

Fig. 2. Histograms for the number of channels with flow rate in a given interval, for values of 0.2 (a) and 0.8 (b) in the standard deviation of the conductance σ_c. The flow at the left is large, and decreases towards the right.

the smallest flow rate is very small for both σ_c. This type of graph will later (Fig. 10) be used to calibrate the model with field data.

The simulations also show that the total flow through the grid increases with increasing σ_c. For example, for $\sigma_c = 2.4$ the flow is 7.4 times larger than for a grid with the same hydraulic conductivity (the same geometric mean) and $\sigma_c = 0$. These values are close to the values predicted for a porous

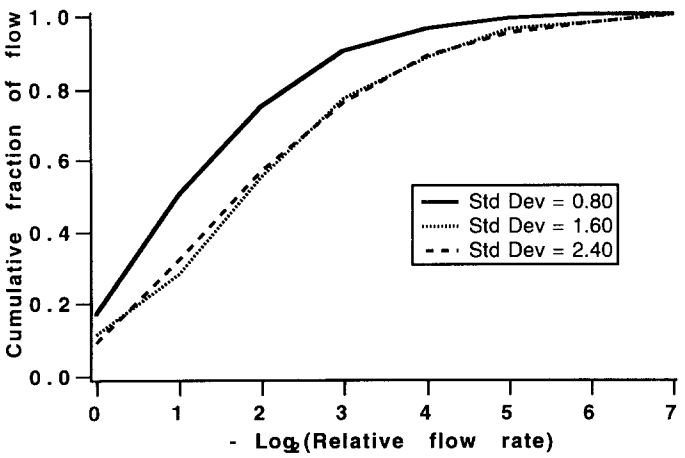

Fig. 3. Cumulative curve for fraction of flow with flow rate less than a given value for different standard deviations in conductances.

medium with variable conductivity (Gelhar and Axness, 1983; Neuman et al., 1987).

The flow rates emerging from the grid have a standard deviation for the logarithmic flow rate of $\sim 0.85\,\sigma_c$. This can be explained by a smoothing effect due to channel connectivity. The smoothing effect is larger for the flow rates inside the grid. When the standard deviation of the flow rates was determined a value of $0.7\,\sigma_c$ was found in the interior of the grid. These results imply that if all flows into a tunnel could be measured, then the standard deviation of the flow-rate distribution would not be equal to that of the flow-rate distribution inside the rock mass.

As shown in Fig. 2, the distribution of the flow rates from the grid, on a logarithmic scale, shows an asymmetric tail extending out to smaller flow rates. This tail is not observed at the field observations because the very small flows are not measured. The measured flow rates cover 2–3 orders of magnitude at most.

Number of "active" channels at intersections

The number of channel members that carry a significant fraction of the total flow will decrease with increasing standard deviation of conductances σ_c. To explore the number of members that contribute significantly to the total flow at each intersection, the following procedure is used.

The curve for conductance distribution (log-normal) is divided into 6 intervals along the axis of log conductances, where each part had the same area under the curve ($\frac{1}{6}$). Then, on average, the member with the smallest conductance in an intersection belongs to the first of these intervals, and the

TABLE 1

Fraction of intersections with a given number of channels, for different standard deviations in the conductance distribution

Number of channels	Standard deviation			
	0.40	0.80	1.60	2.4
0	0.000	0.000	0.004	0.029
1	0.000	0.000	0.033	0.139
2	0.000	0.000	0.130	0.281
3	0.000	0.004	0.268	0.301
4	0.000	0.046	0.316	0.183
5	0.000	0.273	0.199	0.059
6	1.000	0.676	0.052	0.008

member with the largest conductance belongs to the last interval. A conductance that is 1% of the lowest limit of the largest conductance interval (83.3% in the cumulative curve) is considered negligible. The fraction of intersections that has a given number of channel members with non-negligible conductance is then calculated. For example, for a standard deviation σ_c of 1.6, 39% of the members have a conductance less than our limit. From this value, it is found that 5%, 20% and 32% of the intersections have 6, 5 and 4 channels, respectively. 75% of the intersections have $\leqslant 4$ active members. For $\sigma_c = 2.4$, 17% of the intersections have 0 or 1 active channel member, which means that there is no flow there. 28% of the intersections have 2 channel members, which means one conduit. 48% have 3 or 4 channel members and 7% have > 4. Only about half the intersections contribute to mixing processes here. Note that the criterion for non-active channels, $< 1\%$ of the flow in the group of members with the highest flow rates, still includes many members with low flow in the network. A limited number of paths will therefore conduct most of the water flow. These values were checked with simulated results for a grid of $20 \times 20 \times 20$ nodes and the agreement was excellent. Results for different standard deviations are shown in Table 1. The connectivity of the network is strongly reduced when the standard deviation of the conductances is increased. A large standard deviation of conductances results in a network with sparse channel members.

Solute residence time distributions for non-interacting solutes

It will later be demonstrated that the RTD for non-interacting solutes is not and cannot be related to the RTD of sorbing solutes. Nevertheless, non-interacting solutes are commonly used for tracer tests. However, information

on spatial distribution of flow and of mixing and spreading processes in the network can be obtained. For this reason, the RTD properties for non-interacting solutes are discussed here, and some of the limitations in our understanding are pointed out.

Although a limited number of flow paths carries most of the flow, all channel members contribute to some extent. This implies that the distribution of the residence time may become very broad. The fastest paths will be those with large flows, but the tail of the RTD will be determined by low-flow channel members. For large values of σ_c, it may be expected that the difference in residence times between the fast and the slow paths is considerable. The RTD is influenced not only by the flow rates in the channel members but also by their volume.

There are no reliable relationships known, at present, between the conductance and the volume. Several approaches are explored. The volume could be determined from a new *independent distribution* (e.g., a new log-normal distribution). Then the volume of a channel would be totally independent of its conductance. Another choice could be to assume that the aperture is *proportional* to the conductances of the channel members.

The main difficulty in determining which of the possible approaches may represent the volume is the lack of field data. We have tested some approaches between conductance and volume. From these simulations, we expect to find which approach(es) could be used, by comparisons with field observations of the distribution of tracer residence times.

Four approaches were chosen:

(1) Volume assumed to be *proportional* to the hydraulic conductivity, e.g. channels with filling material.

(2) Volume assumed to be *constant*.

(3) Volume proportional to *cubic root* of channel conductance (i.e. proportional to the hydraulic aperture).

(4) Volume determined from an *independent* random distribution.

In the proportional approach, we assume that the conductivity is proportional to the aperture. This would be true if the channel contained filling material that causes the pressure to drop. In the constant approach, a constant volume is assumed. In the cubic root approach, we assume that the aperture is proportional to the conductance raised to an exponent between 0 (constant) and 1 (proportional). The value of the exponent is chosen to be 0.33, in similitude with the cubic law that has been used to describe flow in fractures for a long time. However, there is experimental evidence that this is not true for small aperture channels. The small apertures (constrictions) play an important role in the determination of the conductance, whereas the large apertures determine the volume. Some runs were also done with an exponent of 0.67.

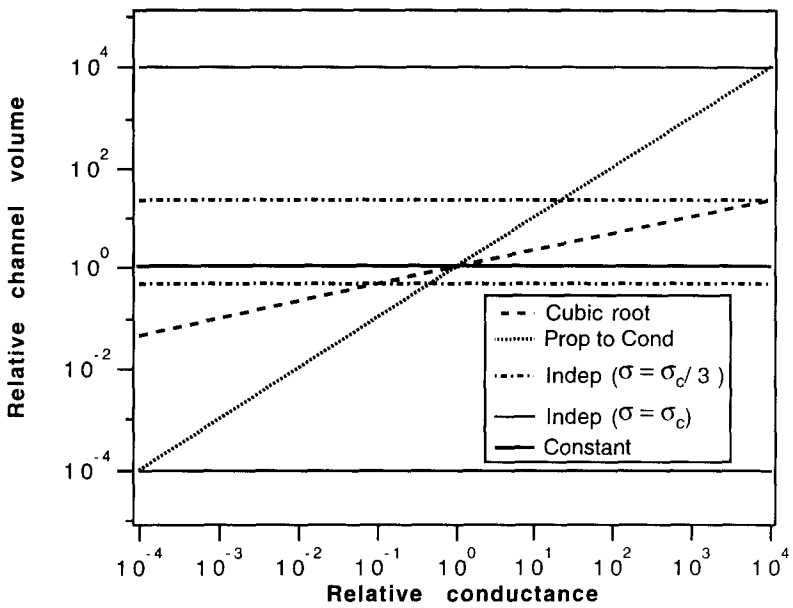

Fig. 4. Channel volume as a function of the channel conductance for the different approaches used in the simulations of solute transport.

In the independent conductance approach, the volumes are randomly generated by assuming that they are log-normally distributed. The standard deviation in the volume distribution is taken to be: (a) $\sigma = \sigma_c/3$ and (b) $\sigma = \sigma_c$.

The interval in which the volume may be found as a function of conductances is compared for the different approaches. For example, for a standard deviation in conductance of 1.2, 95% of the conductances are found within a span of 5 orders of magnitude. Then, for the cubic root approach, the volumes are found in a quite narrow interval ($\sim$ 1.5 orders of magnitude). For the proportional approach, this interval spans 5 orders of magnitude. Fig. 4 shows the relationship between conductance and volume and the possible intervals where volumes may be found for a standard deviation, σ_c, of 1.2.

Two types of injection were used. First, a large number of particles was injected on the high-pressure side of the block and collected on the opposite side. The number of particles that flow into each inlet channel is proportional to the flow rate in these channels. This injection could correspond to the release of contaminants from a repository. This type of injection was chosen because it is independent of the injection location (Moreno et al., 1990).

For the second injection type, many particles are injected at a point in the mesh, and the particles reaching the outlet are collected at their respective

TABLE 2

Péclet number as a function of the standard deviation σ_c for different assumptions used for channel volume

Assumption for channel volume	Standard deviation		
	0.80	1.60	2.40
Proportional to conductance, C	2.63	0.19	0.13
Constant volume	3.90	0.56	0.09
Proportional to $C^{1/3}$	10.45	4.41	1.13
Proportional to $C^{2/3}$	8.41	0.79	0.20
Random with $\sigma = \sigma_c/3$	3.19	0.28	0.80
Random with $\sigma = \sigma_c$	0.41	0.04	0.06

Average values from 20 simulations.

locations. For a mesh of $20 \times 20 \times 20$ nodes, with downward flow, the injection was made at level 15 from the bottom. The mass flow at a given location is proportional to the number of particles that reach that location per unit time. The relative concentration is determined from the number of particles per unit time that arrive at a collection point, divided by the flow rate in the same location. This type of injection was used to compare the data with those from the 3-D tracer test experiment done in Stripa (Abelin et al., 1991a).

Péclet numbers and mean residence times are calculated from the particle residence time distribution. Breakthrough curves corresponding to step injection are also plotted. This is carried out by summation of all the particles that have an arrival time less than a given time.

As will be shown later (Table 5), values of σ_c obtained from comparisons with field observations are in the range of 1.6–2.4.

Péclet numbers when the particles are injected in one of the block sides are shown in Table 2 for different volume approaches. There is insufficient information to accept or reject any of these approaches. However, if we consider that a very large dispersion ($Pe \ll 1.0$) is uncommon in field observations, then some approaches seem less likely, e.g. when the volume is chosen from a new distribution or when the volume of the channel is proportional to the channel conductances. The other approaches give residence time distributions found in field experiments. The largest Péclet number (or the smallest dispersion) is obtained when the channel volume is taken to be proportional to the cubic root of the conductance.

The same results are obtained when point injection is used. The Péclet numbers obtained are shown in Fig. 5 for standard deviations in conductances of 1.6 and 2.4.

The collection sections where the injected tracers (particles) reach the drift

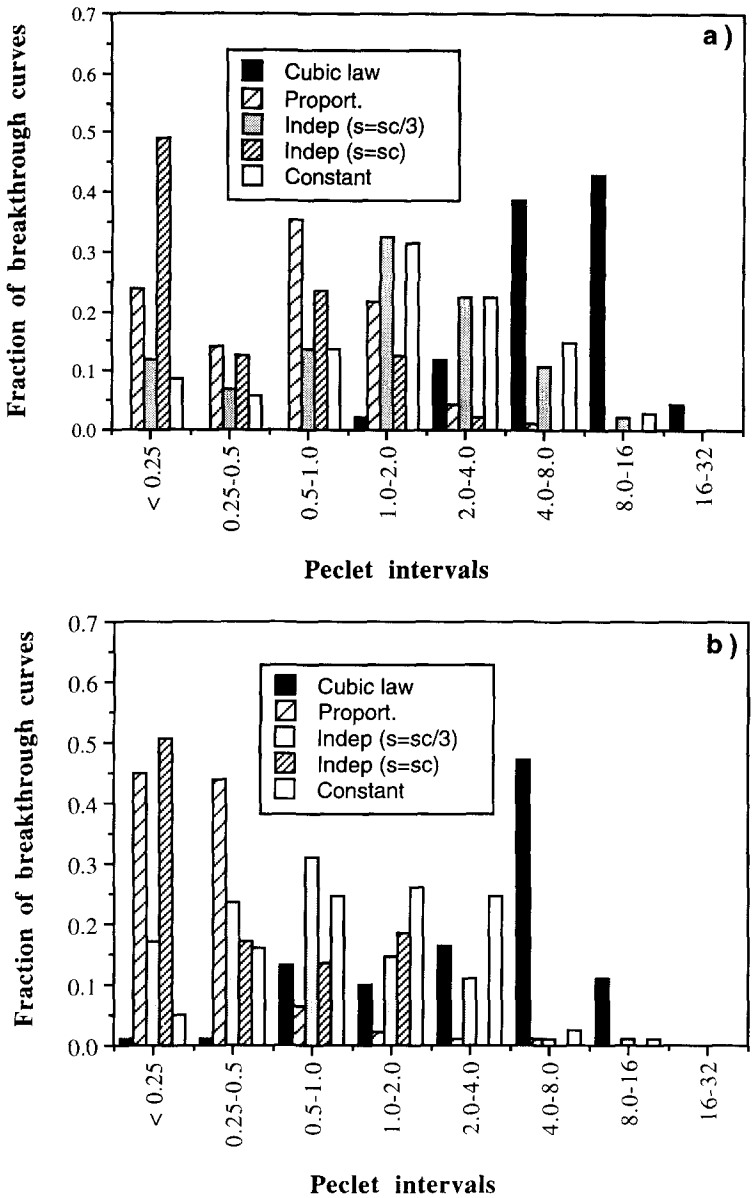

Fig. 5. Histogram showing the Péclet number for standard deviations in channel conductances of 1.6 and 2.4.

are illustrated by plotting their spatial distribution. Fig. 6 shows the maximum concentration at different locations for small ($\sigma_c = 0.2$) and large ($\sigma_c = 1.2$) standard deviations in conductance. When a small standard deviation is used, the spatial distribution of concentration is narrow, with a maximum value under the projected injection point. The concentration decreases rapidly with

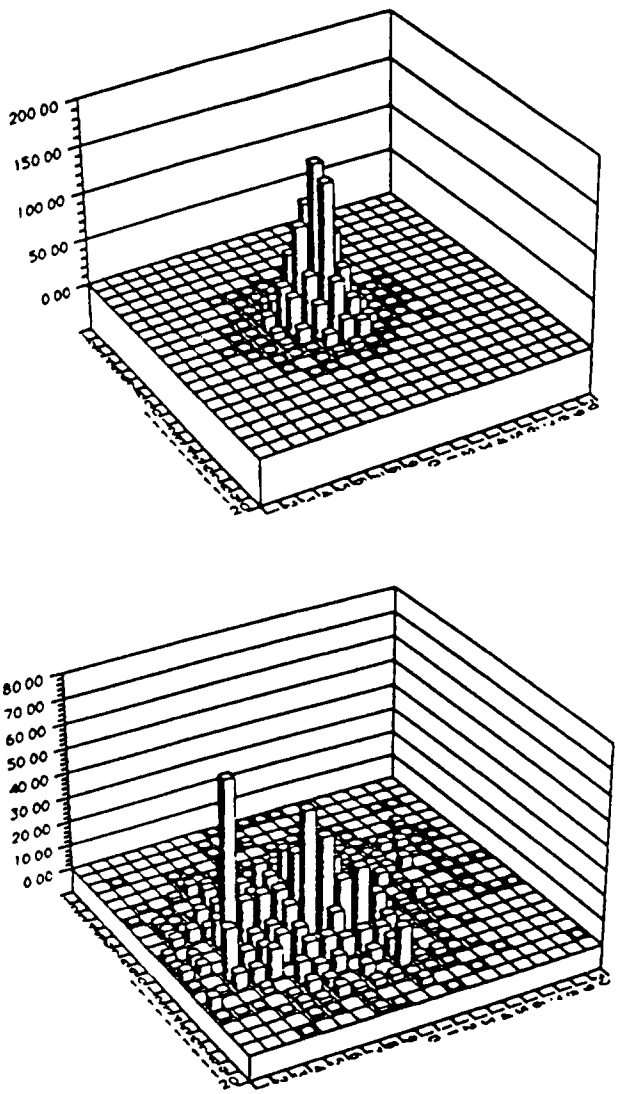

Fig. 6. Spatial distribution of the maximum concentration for a value of 0.2 (a) and 1.2 (b) for the standard deviation of the conductance σ_c. The injection was made in the center of the grid at the level 15 from the bottom for a grid with $20 \times 20 \times 20$ channels

the distance from the projected injection point. For a large standard deviation, the maximum concentration shows some isolated peaks. These results show that the flows in channel members with different conductivities may explain the variations in concentration with the location. Low concentrations may be found surrounded by high concentrations or vice versa. The patterns found in these simulations are similar to those observed in the so-called large-scale experiment at Stripa (Abelin et al., 1991b).

Solute transport for matrix interacting solutes

If the solutes also have access to the matrix porosity by diffusion, the residence times of the solute particles are larger than the residence time without diffusion into the matrix. For low flow rates, Q, in relation to the flow-wetted surface, LW, in a channel member, the solute can be very much retarded compared to the water flow residence time, t_w. In the flow and tracer experiments in Stripa (Abelin et al., 1991b), where water flow residence times for the different tracers varied from months to years, they found that matrix diffusion may have contributed noticeably to the retardation of the tracers. We have therefore incorporated this mechanism in our model for use in later studies of tracer transport.

The residence time for each particle that passes the channel member is stochastically determined by Eq. 6. The capability of the particle following method to describe the diffusion in the rock matrix was tested by generating a network with equal channel members (zero standard deviation). The overall channel thus consists of 15 channel members in series with equal properties. In this channel, we used the stochastic process to simulate the diffusion in the rock matrix. The results agree very well when compared with the analytical solution if a few thousand particles are used. The parameter values were chosen to give no matrix interaction as well as considerable matrix uptake of the tracer. The procedure was found to be fast and accurate also in network calculations as well.

To illustrate the potential impact of matrix diffusion on the transport, a few sample calculations are presented. The data are chosen to be relevant for the migration of a sorbing radionuclide escaping from a deep repository for radioactive waste in granite (SKB, 1992).

Simulations including matrix diffusion were done on a mesh of $20 \times 20 \times 20$ nodes. The member length was assumed to be 5 m; this means a travel distance of 100 m. A channel width of 0.2 m and a channel aperture of 0.1 mm are chosen. The Darcy velocity through the mesh is assumed to be 0.0001 . Therefore the water mean residence time is 2.4 yr. For the product $K_d D_e \rho_p$, which describes the diffusion and sorption properties of the rock, a value of $1.0 \cdot 10^{-10}$ m^2 s^{-1} is assumed. Eq. 6 was determined assuming diffusion into a semi-infinite medium. For sparse channels in crystalline rock, sorbing species penetrate into the matrix only some tens of centimetres in 1 Myr. For nonsorbing species and very long times the penetration fronts from different channels may meet and then the equation is not valid.

The simulations were done with a standard deviation, σ_c, of 1.6. Fig. 7 shows the breakthrough curve for some realizations. The solute transport for species that interact with the matrix is thus determined mainly by the diffusion and sorption properties of the rock, the flow distribution, and the

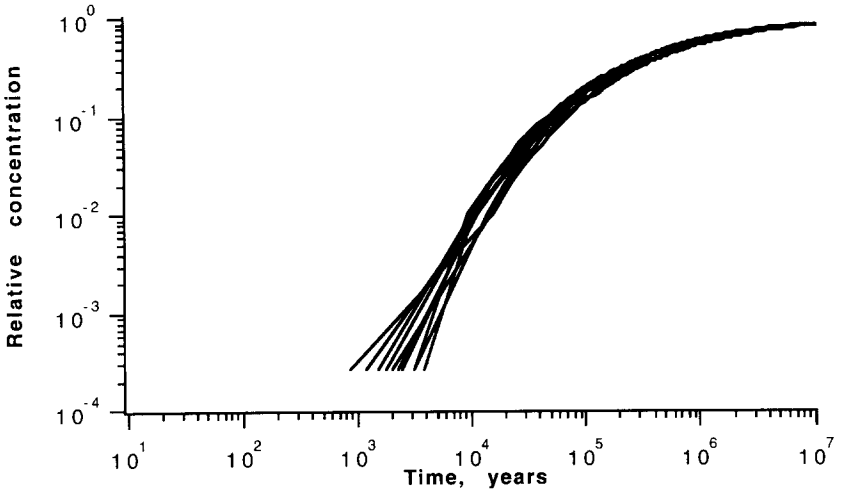

Fig. 7. Breakthrough curves for solutes that interact with the matrix. Water residence time is 2.4 yr.

flow-wetted surface area of the channel. The impact of the channel volume is negligible since the residence time of interacting solutes in a channel is usually much longer than the water residence time, see Eq. 6.

This was also confirmed in the simulations. The breakthrough curves were equal irrespective of the volume–conductance relations used. This suggests that the RTD of tracers that have access to the rock matrix will be determined by the conductance distribution and the flow-wetted surface of the rock, and not by its flow porosity.

To simulate the transport of sorbing solutes which diffuse into and out of the rock matrix, the following data are primarily needed in our model:

— conductance distribution (μ, σ_c)
— channel lengths (L)
— channel widths (W)

The conductance distribution, together with the average hydraulic gradient, gives the flow-rate distribution in the channel network. The channel lengths and widths determine the flow-wetted surface of the channel members. This is sufficient for the simulation of the migration over the distance of interest. Note that no information is needed on flow porosity or "dispersion".

The data needed can be obtained from field observations and experiments. This is done in the next section, where methods are developed to obtain the data from observations and experiments in drifts and tunnels as well as in boreholes.

CALIBRATION AND COMPARISON WITH FIELD OBSERVATIONS

The water inflow to tunnels will be at isolated points on the tunnel walls.

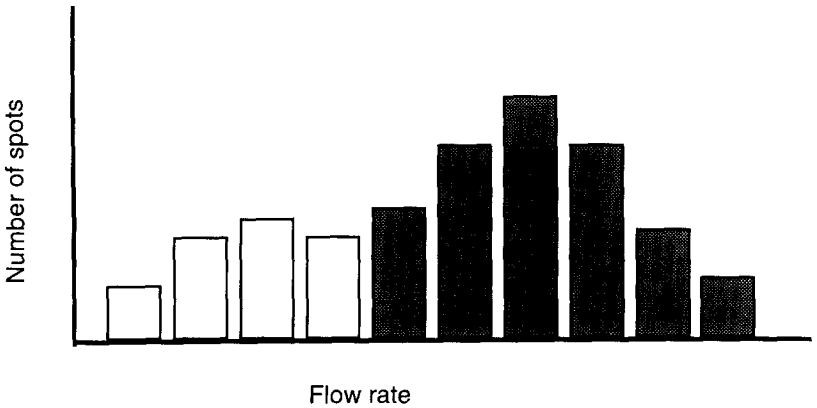

Fig. 8. Histogram showing the number of channels with a flow rate in a given interval. The *shaded bars* represent hypothetical data from field observations. The *white bars* represent channels with a flow rate below the detection limit.

This will look like a number of "channels" being cut by the rock faces of the tunnel. The outflow face of the network model will also have a number of "channels" with flowing water.

The flow rates out from the simulated cubic grid cover a very wide interval, if a large value of σ_c is used. On the other hand, the field results often show variations of only a few orders of magnitude in flow rates. This aspect is schematically presented in Fig. 8. The histogram shows the number of channels with flow rates in a given interval, if even the channels with a very small flow rate could be monitored. From field observations, only data for 6–8 bins may be obtained. They are shown with shaded bars in the figure. The white bars represent the unknown data. The whole histogram could also represent the results of a simulation.

The calibration procedure is as follows. The inflow measurements to the drift are compared with the simulated results. With the available data (the shaded bars) the standard deviation σ_c may be estimated. Then, when the value of σ_c is known, the number of channels in the observable flow-rate interval for the field data is compared with that of the model for the same interval. The total number of channels in the field (observable and non-observable channels or shaded and white bars in the histogram) is obtained by comparing the field data with the results from simulations.

$$\frac{\text{(total number of channels in rock)}}{\text{(total number of channels in simulations)}} = \frac{\text{(number of channels observed in rock above a chosen flow rate)}}{\text{(number of channels in the simulations spanning the same flow-rate range)}} \tag{7}$$

The same procedure can be used for the packer test data in boreholes if these are analysed for the number of intersections, provided channel widths and the borehole diameter are known. This is described in the next section.

The channel network model gives no inherent information on channel member widths or lengths. Nor is the distribution function for the conductances known a priori. If the latter is assumed to be log-normal, then the mean and standard deviation can be found by fitting them to measured data. It has been found, by several investigators, that the standard deviation of transmissivities obtained in boreholes often is between 1 and 3 on a logarithmic (base 10) scale (Cacas et al., 1990a; Geier et al., 1990; Holmes et al., 1990). Dverstorp (1991) used values ranging from 0.4 to 2.4 in simulations of the Stripa experiments with the best results for $\sigma_c = 1.7$. Cacas et al. (1990a) found a value of $\sigma_c = 3.2$ for the Fannay Augère, France, experiments in their fracture network model calibration.

Using data from drifts and tunnels

At the SFR site, there are flow-rate measurements available for individual spots over an area of 14,000 m^2 (Neretnieks, 1987). Table 3 summarizes the data. The flow-rate ranges have been chosen as a decreasing geometrical progression, such that each range "bin" is half the previous one. The reason is that one will undoubtedly observe the largest flow-rate spots, but will have a decreasing accuracy in detecting spots with lower flow rates. It is also generally not possible to know the total inflow to the low-flow-rate spots, so that a cumulative flow-rate curve cannot be constructed to start at the low-flow end. However, a cumulative curve can be started from the high-flow end and can be compared to the model results. If graphs with the cumulative fraction of flow rates are used and the experimental results plotted in those, an estimate of the standard deviation of conductances can be made. The cumulative flow rate increases little when > 5–6 "bins" are used. The method can thus be expected

TABLE 3

Flow rate distribution at the different spots at SFR

Flow rate range	Number of spots	Cumulative number of spots	Fraction of flow rate
⩾1.6	2	2	0.13
0.8–1.6	4	6	0.15
0.4–0.8	12	18	0.21
0.2–0.4	41	59	0.30
0.1–0.2	38	97	0.13
<0.1	67	164	0.08

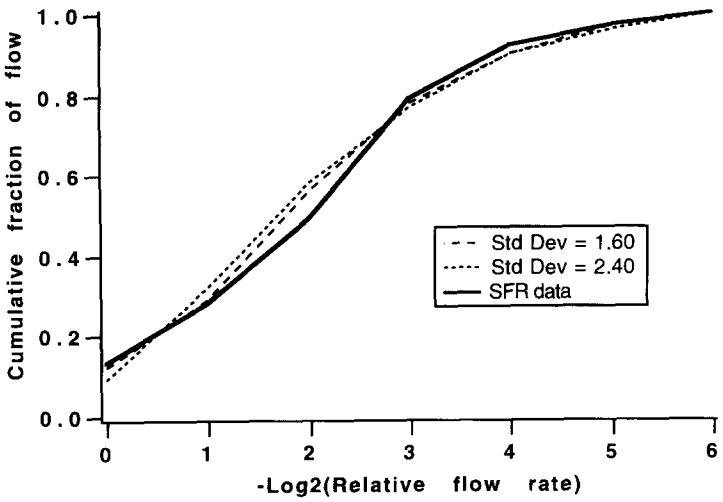

Fig. 9. Cumulative fraction of flow. *Solid line* shows values for SFR data, *dashed lines* show simulated results.

to be robust, in the sense that the most important paths have been accounted for. For the SFR data, σ_c is found to be ~ 1.6 with this method. The cumulative flow-rate curves obtained from the simulations and the cumulative curve from the field observations are shown in Fig. 9. The choice is not totally clear, because the differences between the curve obtained with the SFR observations and the curves for $\sigma_c = 1.6$ and 2.4 are small. For this reason, an alternative procedure is discussed below.

In Table 4, the cumulative number of channels for three σ_c are given. If the ratio of the cumulative number of channels in the model to the number of channels in the SFR observations is calculated, the model and observed results agree best for $\sigma_c = 1.6$. The agreement is based on obtaining the same ratio along the various flow-rate intervals. This is also seen in Fig. 10, where this ratio is plotted as a histogram. The figure shows that the bars for $\sigma_c = 1.6$ are of a more even height than for the other σ_c, meaning that the observed and model distributions agree best for this σ_c. This confirms the value of σ_c obtained with the cumulative flow rates. The values used in Table 3 correspond to average values for 20 realizations.

The values for a grid with 40 channels in each direction are also shown in Table 4. Here, the ratio is also more even for $\sigma_c = 1.6$, indicating that σ_c is not sensitive to the grid size used.

Once σ_c has been established, the number of channels can be found by "aligning" the two columns, "Number of channels in the model" and "Observed number of channels," starting with the highest flow-rate range, see Table 4. The ratio of the number of channels in the model to the observed number of channels was found to be ~ 0.99, which means that the model has

TABLE 4

Match of model and observed flow rates at SFR, for a grid with 20 channels in each direction

Flow rate category	$\sigma_c = 0.8$	$\sigma_c = 1.6$	$\sigma_c = 2.4$	$\sigma_c = 1.6$*	Observed channels at SFR
	Cumulative number of channels from model for				
1	11	2	1	4	2
$\frac{1}{2}$	53	8	6	35	6
$\frac{1}{4}$	119	27	17	114	18
$\frac{1}{8}$	194	57	34	241	59
$\frac{1}{16}$	258	90	56	385	97
$\frac{1}{32}$	351	163	103	685	164
0	400	400	400	1,600	
	Ratio of model to observed channels				
1	5.5	**1.00**	0.5	2.0	
$\frac{1}{2}$	8.8	**1.33**	1.0	5.8	
$\frac{1}{4}$	6.6	**1.50**	0.9	6.3	
$\frac{1}{8}$	3.3	**0.97**	0.6	4.1	
$\frac{1}{16}$	2.7	**0.93**	0.6	4.0	
$\frac{1}{32}$	2.1	**0.99**	0.6	4.2	

Bold face values are for the best fit.
*Grid with 40 channels in each direction.

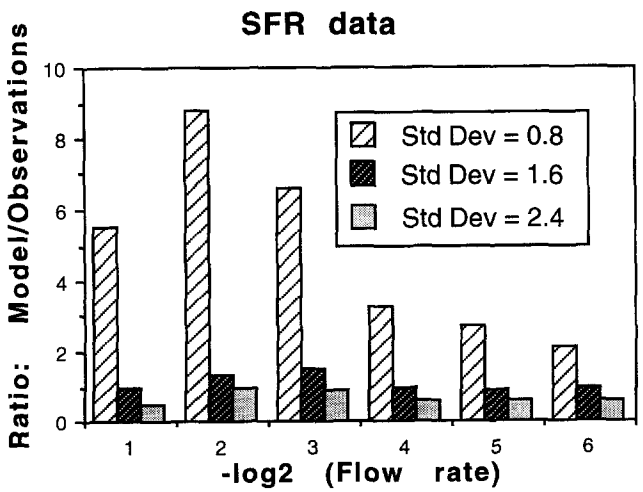

Fig. 10. Ratio of model to observed number of channels in SFR for different standard deviations, σ_c.

TABLE 5

Summary of the results for SFR, Stripa and Kymmen

	σ_c	A (m^2)	Z (drift) (m)
SFR	1.6	35	5.9
Stripa	2.4	2.7	1.6
Kymmen rock mass	2.4	105	10.3
Kymmen zones	2.4	21	4.5

1% fewer channels than the real drifts and cavern at SFR. The model in the present simulations had 400 channels at the outflow face. The SFR thus has $400/0.99 = 404$ inflow channels. In this figure all the channels are included. These 404 channels are found on a surface area of 14,000 m^2. This means that every channel has 35 m^2 on average, and the average length of the channel members is the square root of this figure, $Z = 5.9$ m. When the simulations were done using a grid with 40 channels in each direction, the ratio of the number of channels in the model to the observed number of channels was 4.1. As the total number of channels in the model is 1600, the SFR has 1600/4.1, or 390 inflow channels. This gives a density of 1 channel per 36 m^2 and a length of 6.0 m. The results are only slightly influenced by the grid size.

The same method can be applied to the observations in Stripa, by assuming that every sheet has only one channel. The best agreement is obtained for $\sigma_c = 2.4$. This value is found by matching the model with the observations, for both the cumulative fraction of flow and the cumulative number of channels. The channel density is found to be one channel per 2.7 m^2 and the channel length 1.6 m. Besides the quite detailed Stripa and SFR measurements, there are flow-rate estimates at spots in a drilled tunnel at Kymmen (Neretnieks, 1987). The Kymmen tunnel is a face-drilled tunnel with a length of 4.5 km and a diameter of 4.6 m. 63 fractures zones were identified, which make up a total length of 672 m. Within the rock mass, the channel density is found to be one channel per 105 m^2 and the channel length 10.3 m. For the zones, the area per channel is 21 m^2 and Z is 4.5 m. Table 5 summarizes the results for the three sites.

Channel widths have been measured in drifts and tunnels. Recently Palmqvist and Lindström (1991) analysed earlier observations in the Kymmen tunnel and found that 99.7% of the channels have a width of < 0.1 m. Channel widths at SFR were also a few tens of centimetres, at most, with a few exceptions. A large number of them was point spots, found at fracture intersections and as small holes (Neretnieks, 1987). In the 3-D drift at Stripa, they also found that the water collection sheets collected more water in areas where there were more fracture intersections (Abelin et al., 1991b). A recent

experimental investigation that specifically measured channeling at Stripa (Abelin et al., 1990) also found that channels were typically a few centimeters to a few tens of centimeters wide. We use 10 cm as a "typical" width for channels in this paper.

Using borehole data to estimate channel lengths

In practice, the measurement limit in packer tests determines when a packer section is assumed to be "non-conducting." Typically, the transmissivity of the most conducting sections in the rock mass is 4–6 orders of magnitude more transmissive than the measurement limit. The measurements are usually available in the form of a number of packer intervals with measured transmissivities for the borehole tests. These measurements can be used to estimate the total number of conductive fractures (channels) intersected by the borehole(s). This has been done on data from Stripa (Geier et al., 1990). The information then needs to be translated into the number of channels of a given width W and length Z per rock volume. A method for doing this is developed below.

The rock contains a large number of channels randomly orientated, with an average length Z and an average width W. If there are several of such channels in a volume of rock, a borehole that is drilled in the rock may intersect some of them. In this analysis, we assume that the aperture of the channels is very small compared to the other dimensions of the channels and

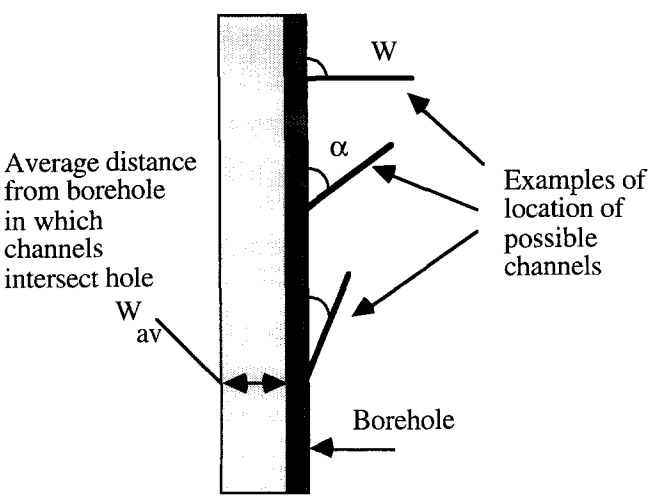

Fig. 11. The average distance at which the "outside" of the channel can be situated and still touch the borehole. W is the width of the channel and α is the intersection angle between the borehole and the channel.

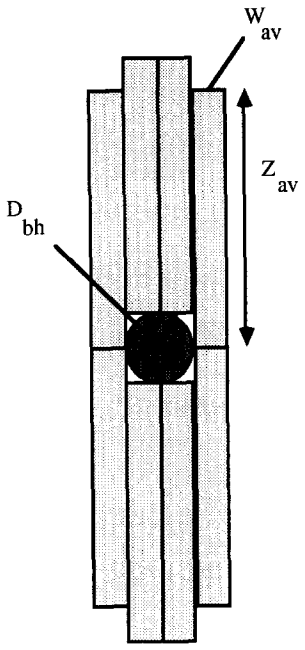

Fig. 12. View of borehole from above, indicating at what distance from the borehole a channel must lie, on average, in order to be in contact with a borehole.

that the widths of the channels are small in relation to the average distance between channels.

Consider a borehole with diameter D_{bh} and how a channel must be located in order to be in contact with the hole. Fig. 11 shows a vertical borehole and a channel with different angles to the horizontal. The average distance, W_{av}, is obtained by integrating over all angles α:

$$W_{av} = \tfrac{1}{2}\pi^{-1} \int_0^{\frac{1}{2}\pi} W \sin\alpha \mathrm{d}\alpha = W 2\pi^{-1} \tag{8}$$

In the same way the average distance at which a channel will intersect the hole in the other direction, Z_{av}, can be obtained. This is illustrated in Fig. 12.

$$Z_{av} = \tfrac{1}{2}\pi^{-1} \int_0^{\frac{1}{2}\pi} Z \sin\beta d\beta = Z 2\pi^{-1} \tag{9}$$

Thus the average area in Fig. 12 in which a channel must lie to contact the hole is:

$$A_{av} = \tfrac{1}{4}\pi D_{bh}^2 + 2Z_{av}(D_{bh} + 2W_{av}) \tag{10}$$

If the average distance between channels intersected by the borehole has been shown to be H, then the rock volume containing one channel is HA_{av}. In a system with a cubic grid of channels, every cube with sides Z is delimited by 12

channels. Every channel is shared by four other cubes, so there are three channels per volume of size Z^3. Thus:

$$Z^3 = 3HA_{av} = 3H[\tfrac{1}{4}\pi D_{bh}^2 + 2Z_{av}(D_{bh} + 2W_{av})] \tag{11}$$

Substituting Eqs. 8 and 9 into Eq. 11 gives:

$$Z^3 = 3H[\tfrac{1}{4}\pi D_{bh}^2 + 4Z\pi^{-1}(D_{bh} + 4W\pi^{-1})] \tag{12}$$

If H, D_{bh} and W are known from independent measurements, then Z is obtained from Eq. 12. When $Z \gg D_{bh}$, the first term in Eq. 12 can be neglected and Z is obtained from:

$$Z^2 = H12\pi^{-1}(D_{bh} + 4W\pi^{-1}) \tag{13}$$

Geier et al. (1990) found that in three horizontal north–south-orientated boreholes, drilled nearly parallel to the 3-D drift in Stripa, the standard deviation of transmissivities was 1.5 a logarithmic (base 10) scale and the conductive fracture frequency was 0.57 m^{-1}. This fracture frequency corresponds to the total number of conductive fractures. In two horizontal east–west-orientated boreholes, starting at the 3-D drift, the same values were found for the fracture density and the standard deviation. The mean transmissivity, however, was 10 times higher in the latter holes.

With a width $W = 0.1$ m and a borehole diameter of 0.076 m, Eq. 13 above gives an average channel grid length Z of 1.2 m. This agrees reasonably well with the results obtained from the observations of flow-rate distribution in the 3-D drift, where Z was 1.6 m.

Thus measurements from drifts and tunnels as well as from boreholes can be used to estimate the channel lengths. To use borehole information, channel widths are needed. However, the results are not very sensitive to the channel widths if they are of the same magnitude as the borehole diameter. This can be seen from Eq. 13. If W is taken to be equal to D_{bh} (although it is much less in reality), Z would have been overestimated by 51%. This is not a very large error compared to many other entities used for the simulation of flow in the network. However, W has a large effect on the interacting tracers, because it directly influences the flow-wetted surface. It must, for this reason, be determined accurately. We have found very few measurements, beyond those mentioned, that could be used to determine the flow-wetted surface or channel width more precisely.

In the next subsection, an attempt is made to use some tracer data to at least check if the value $W \approx 0.1$ m is at all reasonable.

Using residence time distributions from tracer tests

The Stripa tracer experiments also gave information on the porosity, which

was in the range $(0.2–1.5)\cdot10^{-4}$ for the different tracers. The average was $0.6\cdot10^{-4}$. The porosity of our model rock is:

$$\epsilon_f = 3Wb/Z^2 \tag{14}$$

With channels 0.1 m wide and 0.1 mm in aperture, the porosity of our rectangular grid is $0.2\cdot10^{-4}$ for $Z = 1.2$ m and $0.1\cdot10^{-4}$ for $Z = 1.6$ m. Since the aperture and the width are not fully determined, the similarity may be chance.

The Stripa tracer experiments were also analysed for matrix diffusion effects, and the "flow-wetted surface" was estimated to vary between 0.2 and 2 $m^2\ m^{-3}$, possibly up to 20 $m^2\ m^{-3}$, for the various tracers. The flow-wetted surface area in the model grid is:

$$a = 6W/Z^2 \tag{15}$$

The value of a is 0.4 $m^2\ m^{-3}$ for $Z = 1.2$ and 0.2 $m^2\ m^{-3}$ for $Z = 1.6$ m. The values fall within the range measured in the actual field experiment, but the uncertainties are too large at present to draw any firm conclusions.

DISCUSSION AND CONCLUSIONS

The model proposed is intentionally made simple so that it is easy to incorporate tracer transport and to accommodate interacting tracers. The model must be calibrated to field measurements. Borehole transmissivity data obtained by "narrow" packer intervals should, in principle, suffice to obtain the effective channel lengths, provided channel widths can be determined independently. The comparisons and calibrations with field observations are rather straightforward and have shown that the model can exhibit the properties of channeling observed in the field. Tracer residence time distributions and patterns also agree.

The fair agreement between the predicted flow porosity and the flow-wetted surface area, found in the Stripa experiments, cannot by itself be used as a basis for model acceptance. Although encouraging, more comparisons with field tracer tests are needed.

It has been demonstrated that the flow-wetted surface area is of prime importance for the migration of solutes which diffuse into the rock matrix. This applies to solutes such as dissolved radionuclides. There are not enough detailed in situ observations that can be used to assess the flow-wetted surface area. Special techniques and tests must be developed and applied to obtain more accurate information.

REFERENCES

Abelin, H., Neretnieks, I., Tunbrant, S. and Moreno, L., 1985. Final report of the migration in a single fracture — Experimental results and evaluation. OECD/NEA (Org. Econ. Coop. Dev./Nucl. Energy Agency), SKB (Swed. Nucl. Fuel&Waste Manage. Co.), Stockholm, Stripa Proj. Tech. Rep. 85-03, 102 pp.*

Abelin, H., Birgersson, L., Widén, H., Ågren, T., Moreno, L. and Neretnieks, I., 1990. Channeling experiment to study flow and transport in natural fractures. OECD/NEA (Org. Econ. Coop. Dev./Nucl. Energy Agency), SKB (Swed. Nucl. Fuel&Waste Manage. Co.), Stockholm, Stripa Proj. Tech. Rep. 90-13, 144 pp.*

Abelin, H., Birgersson, L., Gidlund, J. and Neretnieks, I., 1991a. A large-scale flow and tracer experiment in granite, 1. Experimental design and flow distribution. Water Resour. Res., 27: 3107–3117.

Abelin, H., Birgersson, L., Moreno, L., Widén, H., Ågren, T. and Neretnieks, I., 1991b. A large-scale flow and tracer experiment in granite, 1. Results and interpretation. Water Resour. Res., 27: 3119–3135.

Cacas, M.C., de Marsily, G., Tillie, B., Barbreau, A., Durand, E., Feuga, B. and Peaudecerf, P., 1990a. Modelling fracture flow with a stochastic discrete fracture network: calibration and validation, 1. The flow model. Water Resour. Res., 26: 479–489.

Cacas, M.C., Ledoux, E., de Marsily, G., Barbreau, A., Calmels, P., Gaillard, B. and Margritta, R., 1990b. Modelling fracture flow with a stochastic discrete fracture network: calibration and validation, 2. The transport model. Water Resour. Res., 26: 491–500.

Carslaw, H.S. and Jaeger, J.C., 1959. Conduction of Heat in Solids. Oxford University Press, Oxford, 2nd ed., 510 pp.

Dershowitz, W., Wallmann, P. and Kindred, S., 1991. Discrete fracture modelling for the Stripa site characterization and validation drift inflow predictions. OECD/NEA (Org. Econ. Coop. Dev./Nucl. Energy Agency), SKB (Swed. Nucl. Fuel&Waste Manage. Co.), Stockholm, Stripa Proj. Tech. Rep. 91-16, 100 pp.*

Dverstorp, B., 1991. Analyzing flow and transport in fractured rock using the discrete fracture network concept. Ph.D. Thesis, Department of Hydraulic Engineering, Royal Institute of Technology, Stockholm, TRITA-VBI-151, 31 pp.

Dverstorp, B. and Andersson, J., 1989. Application of the discrete fracture network concept with field data: Possibilities of model calibration and validation. Water Resour. Res., 25(3): 540–550.

Geier, J., Dershowitz, W. and Sharp, G., 1990. Prediction of inflow into the D-holes in the Stripa mine. OECD/NEA (Org. Econ. Coop. Dev./Nucl. Energy Agency), SKB (Swed. Nucl. Fuel&Waste Manage. Co.), Stockholm, Stripa Proj. Tech. Rep. 90-06, 76 pp.*

Gelhar, L.W. and Axness, C.L., 1983. Three-dimensional stochastic analysis of macrodispersion in aquifers. Water Resour. Res., 19(1): 161–180.

Herbert, A. and Splawski, B., 1990. Prediction of inflow into the D-holes at the Stripa mine. OECD/NEA (Org. Econ. Coop. Dev./Nucl. Energy Agency), SKB (Swed. Nucl. Fuel&Waste Manage. Co.), Stockholm, Stripa Proj. Tech. Rep. 90-14, 72 pp.*

Herbert, A., Gale, B.J., Lanyon, G. and MacLeod, R., 1991. Modelling for the Stripa site characterization and validation drift inflow: Prediction of flow through fractured rock. OECD/NEA (Org. Econ. Coop. Dev./Nucl. Energy Agency), SKB (Swed. Nucl. Fuel&Waste Manage. Co.), Stockholm, Stripa Proj. Tech. Rep. 91-35, 161 pp.*

*KBS/SKB — Technical Reports can be obtained from: INIS Clearing House, International Atomic Energy Agency, P.O. Box 100, A-1400 Vienna, Austria.

Holmes, D., Abbot, M. and Brightman, M., 1990. Site characterization and validation — Single borehole hydraulic testing of "C" boreholes, simulated drift experiments and small scale hydraulic testing, Stage *3*. OECD/NEA (Org. Econ. Coop. Dev./Nucl. Energy Agency), SKB (Swed. Nucl. Fuel&Waste Manage. Co.), Stockholm, Stripa Proj. Tech. Rep. 90-10, 90 pp.*

Levenspiel, O., 1972. Chemical Reaction Engineering. Wiley, New York, NY, 2nd ed., 566 pp.

Long, J.C.S., Endo, H.K., Karasaki, K., Pyrak, L., MacLean, P. and Witherspoon, P.A., 1985. Hydrological behavior of fracture networks. Int. Assoc. Hydrogeol. Conf. on Hydrogeology of Rocks of Low Permeability, Tucson, AZ, Jan. 7–10, 1985, 17: 449–462.

Moreno, L., Tsang, Y.W., Tsang, C.F., Hale, F.V. and Neretnieks, I., 1988. Flow and tracer transport in a single fracture — A stochastic model and its relation to some field observations. Water Resour. Res., 24: 2033–2048.

Moreno, L., Tsang, C.F., Tsang, Y.W. and Neretnieks, I., 1990. Some anomalous features of flow and solute transport arising from fracture aperture variability. Water Resour. Res., 26: 2377–2391.

Neretnieks, I., 1980. Diffusion in the rock matrix: An important factor in radionuclide retardation? J. Geophys. Res., 85: 4379–4397.

Neretnieks, I., 1987. Channeling effects in flow and transport in fractured rocks — Some recent observations and models. Pap. presented at GEOVAL Symp., Stockholm, Proc., pp. 315–335.

Neretnieks, I., Abelin, H. and Birgersson, L., 1987. Some recent observations of channeling in fractured rocks — Its potential impact on radionuclide migration. U.S. Dep. Energy–At. Energy Can. Ltd. Conf., San Francisco, CA, Sept. 15–17, 1987, Proc., pp. 387–410.

Neuman, S.P., Winter, C.L. and Newman, C.M., 1987. Stochastic theory of field-scale dispersion in anisotropic porous media. Water Resour. Res., 23(3): 453–466.

Palmqvist, K. and Lindström, M., 1991. Channel widths. SKB (Swed. Nucl. Fuel&Waste Manage. Co.), Stockholm, Tech. Rep. TR 91-14, 11 pp.*

Palmqvist, K. and Stanfors, R., 1987. The Kymmen power station TBM tunnel — Hydrogeological mapping and analysis. SKB (Swed. Nucl. Fuel&Waste Manage. Co.), Stockholm, Tech. Rep. TR 87-26, 18 pp.*

Robinson, P.C., 1984. Connectivity, flow and transport in network models of fractured media. Ph.D. Thesis, St. Catherine's College, Oxford University, Oxford, Ref. TP 1072, 118 pp.

SKB (Swedish Nuclear Fuel and Waste Management Company), 1992. Final disposal of spent nuclear fuel — Importance of the bedrock for safety. SKB (Swed. Nucl. Fuel&Waste Manage. Co.), Stokholm, Tech. Rep. TR 92-20, SKB-91, 197 pp.*

Smith, L., Schwartz, F. and Mase, C., 1987. Applications of stochastic methods for the simulation of solute transport in discrete and continuum models of fractured rock systems. Proc. Conf. on Geostatistical, Sensitivity and Uncertainty Methods for Ground-Water Flow and Radionuclide Transport Modelling, San Francisco, CA, Sept. 15–17, 1987, pp. 425–440.

Yamashita, R. and Kimura, H., 1990. Particle-tracking technique for nuclide decay chain transport in fractured porous media. J. Nucl. Sci. Technol., 27: 1041–1049.

*KBS/SKB — Technical Reports can be obtained from: INIS Clearing House, International Atomic Energy Agency, P.O. Box 100, A-1400 Vienna, Austria.